Thermal Evolution of Acetic Acid Nanodeposits over 123−180 K on Noncrystalline Ice and Polycrystalline Ice Studied by FTIR Reflection−Absorption Spectroscopy: Hydrogen-bonding Interactions in Acetic Acid and between Acetic Acid and Ice

Q. Gao and K. T. Leung*

Department of Chemistry, University of Waterloo, Waterloo, Ontario N2L 3G1, Canada

Received: March 29, 2005; In Final Form: May 10, 2005

Acetic acid vapor-deposited on ultrathin noncrystalline ice (NCI) and polycrystalline ice (PCI) films (less than 6 nm thick) under ultrahigh vacuum conditions has been investigated by using Fourier Transform Infrared Reflection−Absorption Spectroscopy. Pristine acetic acid deposited at 123 K (on a copper support) appears as an amorphous solid, which undergoes an irreversible phase transformation to a more structurally ordered (polycrystalline) form upon annealing to 153 K. Acetic acid is found to adsorb on NCI and PCI films initially through hydrogen bonding between C=O and dangling OH (of ice), followed by the formation of multilayers at 123 K. Thermal evolution studies of a low exposure of acetic acid on the ultrathin NCI and PCI films show that acetic acid undergoes coevaporation with water likely as an acetic acid hydrate at 155 K, which continues until the entire ice film has been exhausted at 165 K. Above 165 K, the remaining acetic acid solid appears to evaporate without undergoing the phase transformation, in contrast to the case of a high acetic acid exposure. Coevaporation of acetic acid with water is also found to proceed at a faster rate than the subsequent evaporation of acetic acid, which is consistent with the weaker interactions observed in the H-bonded acetic acid hydrate than that in acetic acid solid.

1. Introduction

Ice has attracted a lot of attention over the past decade due to the relevance of its surface chemistry to heterogeneous processes found in atmospheric sciences, environmental studies, and planetary research.[1,2] For example, reactions on the surfaces of stratospheric cloud particles play a key role in the formation of the ozone hole over Antarctica.[3] Heterogeneous processes on aerosol particles could also be responsible for such atmospheric processes as the tropospheric scavenging of ozone in the Arctic[4,5] and the enhanced midlatitude depletion of ozone.[6,7] Oxygenated hydrocarbons (including acetaldehyde, acetone, and acetic acid) are particularly important in atmospheric chemistry because they can be easily decomposed to form hydroxyl radicals that are found to be responsible for ozone depletion in the atmosphere.[8] The study of the uptake or adsorption of oxygenated hydrocarbons in clouds (and in particular on ice particles) and other atmospheric particulates could provide new insights into the heterogeneous chemistry of clouds related to climate change and other environmental issues.[9]

Previous studies have shown that the adsorption of a guest molecule on ice is sensitive to the nature of the guest molecule and the interfacial sites, and the types and extent of the corresponding interactions can be probed by using infrared spectroscopy.[10−13] These results have been based upon the frequencies observed for the OH dangling bond of water molecules.[13] In the solid forms, water is considered to form four hydrogen bonds to other water molecules following the so-called ice rule,[14] but the coordination sites of the water molecules in the case of noncrystalline ice (NCI) may not be fully saturated. Devlin and co-workers have shown that these sites give rise to two IR bands at 3720 and 3696 cm^{-1}, corresponding to doubly

coordinated and triply coordinated water molecules, respectively.[15,16] These OH dangling-bond features are found to be very weak in comparison to the OH stretch feature of bulk ice (3800−2800 cm^{-1}) and are sensitive to the types of interactions with other molecules. For example, the study of the adsorption of hydrogen and nitrogen on NCI by Rowland et al. has revealed red shifts of 10 cm^{-1} in these dangling-bond features for doubly coordinated and triply coordinated adsorption sites.[13] In the case when strong H-bonding is involved in the adsorption of a guest species, the red shift in the OH dangling bond is expected to increase.[12] The weak OH dangling-bond feature for a guest species (e.g., acetone) upon adsorption on ice could then be obscured by the much stronger OH stretch feature of the bulk if the magnitude of the red-shift happens to be large.[12] Moreover, the CO stretch of carbon monoxide adsorbed on NCI was found to be a doublet at 2153 and 2137 cm^{-1}, corresponding to adsorption at two different types of sites.[10] The band at 2153 cm^{-1} is found to locate at a similar position to those of the corresponding CO stretch for CO complexes with HF, HCl, and HBr at low temperature (12 K),[17] in which CO acts as a proton acceptor to the OH dangling bond of the ice substrate. The effects of adsorption of more complicated molecules (polyatomics) have also been studied on ice surfaces.[11] In particular, Horn et al. observed that the red shifts in the OH dangling-bond features appear to increase with increasing Cl content in the chlorofluorocarbon series (i.e., CCl_2F_2 < CCl_3F < CCl_4).[11] The magnitudes of the observed red shifts were further found to show a strong correlation with a number of physicochemical parameters including the molecular polarizability and the C−Cl bond dissociation energy.[11] However, the limited number of compounds surveyed by Horn et al.[11] did not allow any general conclusions to be made.

Acetic acid (CH_3COOH) is one of the simpler organic acids that is commonly used as a benchmark for comparison with

---

* Address correspondence to this author. E-mail: tong@uwaterloo.ca.

small inorganic acids (including HF and HCl[18]) that have been under intense investigation in atmospheric research. As a guest species on ice, acetic acid is fundamentally interesting because the carbonyl and hydroxyl groups can interact with the water molecules on the ice surface through H-bonding interactions with the hydrogen atom in the OH dangling bond and with the dangling O atom, respectively. We have previously studied the adsorption of acetone (CH_3COCH_3) on ice by using FTIR Reflection−Absorption Spectroscopy (FTIR-RAS),[19] which together with the present study on acetic acid could provide an extended database for contrasting the effects of the hydroxyl groups on the ice surface chemistry. Unlike formic acid (HCOOH), acetic acid is also less likely to form dimers at room temperature and it is therefore easier to handle experimentally.

To date, only a few studies have been reported for the adsorption of acetic acid on ice and no corresponding spectroscopic data are available in the literature. In particular, Hudson et al. have measured the uptake of a series of gaseous organic molecules (acetone, acetaldehyde, acetic acid) on ice below 200 K,[20] and their results show that acetic acid is bound strongly to the ice surface. Sokolov and Abbatt have also studied the adsorption of *n*-alcohols, acetic acid, and hexanal between 213 and 245 K.[21] From concentration analyses of ice samples, Guerinot found that acetic acid exists in its molecular form.[22] In addition, Compoint et al. compared the adsorption geometries and dynamics of acetic acid on/in ice with those of formic acid at 250 K by classical molecular dynamics simulation,[23] and they found that acetic acid is bound to the ice surface through the formation of two hydrogen bonds that are influenced only slightly by the steric packing of the methyl group. Furthermore, the calculated free energy profiles show that acetic acid is strongly trapped at the surface of ice at 250 K. Relative to molecular desorption, the penetration of acetic acid into ice at 250 K should be more favorable, because the corresponding penetration barrier is two or three times smaller than the desorption barrier.[23] The present work focuses on the interactions of acetic acid with ultrathin NCI and polycrystalline ice (PCI) films by using FTIR-RAS. In addition to the aforementioned interest, acetic acid is also a convenient guest molecule for probing the ice surface chemistry spectroscopically because its chemistry on metal surfaces is well documented[24] and the gas-phase infrared spectrum has been characterized, facilitating easy comparison with the present work.

2. Experimental Details

Details of the experimental setup and procedure have been discussed elsewhere.[25] Briefly, the FTIR-RAS experiments were performed in an ultrahigh-vacuum (UHV) chamber evacuated by a 170 l s^{-1} turbomolecular pump and a titanium sublimation pump to a base pressure better than 3.0×10^{-9} Torr. A vertically mounted, optically flat polycrystalline OFHC copper disk (5.7-cm diameter) directly attached to a liquid nitrogen cooled dewar was used for film growth by vapor deposition. The liquid nitrogen cooled dewar also served as a cryopump reducing the chamber pressure to 5.0×10^{-10} Torr during the experiments. The temperature of the sample on the copper disk could be varied by using a resistance heater imbedded in the backside of the copper disk under the control of a temperature controller. The relative temperature measurement was obtained by using two K-type (chromel−alumel) thermocouples mechanically fastened to the front face of the disk to a precision of better than ±2 K, while the uniformity of the temperature across the disk surface was expected to be better than 5 K. To ensure a highly conductive surface with good deposition reproducibility,

the copper disk was precleaned before the vapor deposition by sputtering with argon ions at 1.5 keV impact energy at 5.0×10^{-6} Torr for 30 min.

The infrared beam from a Bruker Equinox 55 FTIR spectrometer (equipped with an air-cooled Globar source) was directed at the condensed sample on the copper disk by a 45° flat mirror followed by a 90° refocusing parabolic mirror (with a 40-cm focal length). The IR beam specularly reflected off the sample at 83° from the surface normal was collected by a second identical parabolic mirror (40-cm focal length) located at the opposite side of the chamber, and finally focused by a smaller parabolic mirror (4.3-cm focal length) onto a liquid nitrogen cooled Mercury Cadmium Telluride detector (energy range: 7000−600 cm^{-1}; sensitivity $>2.5 \times 10^{10}$ cm Hz$^{1/2}$ W^{-1}). Two differentially pumped CaF_2 optical windows are mounted on the UHV chamber to enable the IR beam to pass through and intersect with the sample. The optical path along the mirror optics outside the UHV chamber was enclosed in aluminum boxes and purged with dry nitrogen gas to remove spectral interference due to water vapor and carbon dioxide in the ambient environment.

FTIR-RA spectra of the deposited sample were obtained over the spectral range of 1000−4000 cm^{-1} by coadding 20 scans at 20 kHz scanner frequency at a preset spectral resolution of 1 cm^{-1}. Background spectra were collected for the bare copper disk at the deposition temperature (before the vapor deposition) by coadding 500 scans at the same resolution setting and were later removed from the spectra collected for the deposited sample. The resulting background-subtracted sample spectra were then presented in the dimensionless absorbance unit, defined as $-\log(R/R_0)$, where R/R_0 is the ratio of the reflectance of the substrate with and without the adsorbate. The difference of two background-subtracted sample spectra, denoted as difference spectra in the present work, was used to reveal spectral features corresponding to the changes in the deposition process.

Vapors of water (Millipore) and acetic acid (Aldrich, 99.7% purity) were introduced into the chamber separately through variable precision leak valves after the respective liquid samples have been degassed by several freeze−pump−thaw cycles. Different amounts of acetic acid (in units of Langmuir, 1 L = 1×10^{-6} Torr s) were deposited on an ice film with a pre-selected film thickness by exposing the film at an appropriate deposition pressure accumulatively for different periods of exposure time. The thickness of the ice film was estimated by using a procedure based on the Fresnel method, which has been given in detail in our previous work.[25]

3. Results and Discussion

3.1. Preparation and Characterization of Noncrystalline and Polycrystalline Ice Films. Figure 1a shows the FTIR-RA spectrum of an ice film deposited at 5.0×10^{-7} Torr for 900 s at 123 K, which is estimated to have a film thickness of ∼6 nm from the Fresnel analysis.[25] Evidently, the spectrum is dominated by a strong broad band at 3376 cm^{-1} and a weaker feature at 1656 cm^{-1}, corresponding to the OH stretching modes and the HOH bending mode of the bulk, respectively. Furthermore, a sharp but considerably weaker feature at 3696 cm^{-1} can also be observed, which can be attributed to the OH dangling-bond mode, i.e., the OH stretching mode for which the H atom is not involved in the H-bonding. The spectral assignments are consistent with those made for a thin NCI film.[15,16,26] The observed spectrum (Figure 1a) also closely resembles the transmission spectrum of a liquid water film at

Thermal Evolution of Acetic Acid Nanodeposits

J. Phys. Chem. B, Vol. 109, No. 27, 2005 **13265**
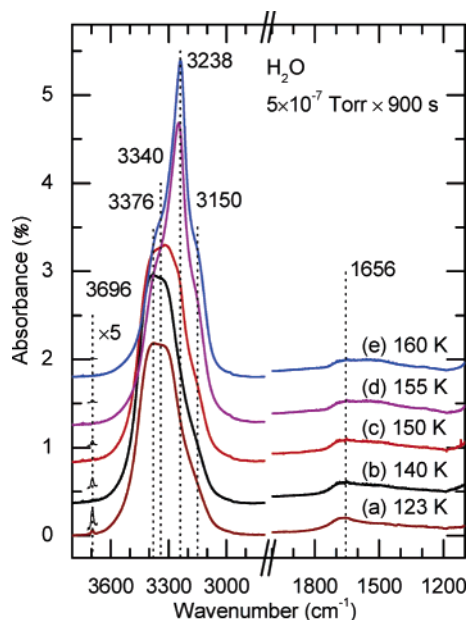
Figure 1. FTIR-RA spectra of (a) an noncrystalline ice film (∼6 nm thick) vapor-deposited at 5 × 10⁻⁷ Torr for 900 s at 123 K, and upon annealing to (b) 140, (c) 150, (d) 155, and (e) 160 K. The conversion to polycrystalline ice film is complete at 160 K.
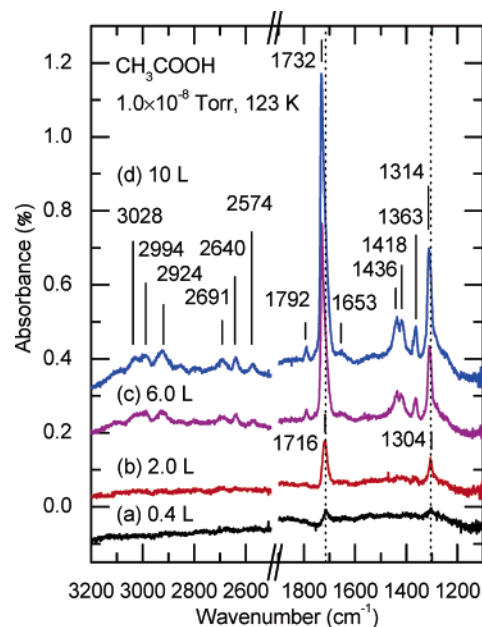

Figure 2. FTIR-RA spectra of acetic acid vapor-deposited at 1.0 × 10⁻⁸ Torr at 123 K as a function of exposure: (a) 0.4, (b) 2.0, (c) 6.0, and (d) 10 L.

room temperature (with the exception of the OH dangling-bond feature at 3696 cm⁻¹), which further confirms the amorphous nature of the ice film.[27]

Figure 1 also shows the spectral evolution of the NCI film upon annealing to 160 K. In particular, the bulk OH stretching feature appears as a sharp peak at 3238 cm⁻¹, while the intensities of the bulk HOH bending modes (at 1656 cm⁻¹) and the OH dangling-bond mode (at 3696 cm⁻¹) are found to decrease (Figure 1e). These spectral changes observed at 160 K are consistent with those observed for a PCI film.[28,29] Detailed discussion of the temporal evolution of NCI upon annealing to PCI has been given in our recent work.[29] As shown in Figure 1, both NCI and PCI films exhibit characteristic spectral features that can be used as fingerprints for easy identification. For the purpose of the present work, we prepared an NCI film by water vapor deposition at 123 K, which was then used to obtain a PCI film by annealing to 160−165 K for 5 min.

3.2. Characterization of Pristine Acetic Acid Solid Films. Acetic acid can exist in several different forms in the condensed phase. In the liquid phase, acetic acid primarily exists as cyclic dimers,[30] while evidence for open-chain dimers has also been reported.[31] In the solid phase, acetic acid has been found to exist as a chainlike polymer.[32,33] The C=O stretching vibration in acetic acid is found to be particularly sensitive to the different physical forms of acetic acid. In particular, while this vibrational mode occurs at 1788 and 1730 cm⁻¹ respectively for the monomer[32] and dimer in the gas phase,[34] it is found to shift to 1715 cm¹ for the cyclic dimer in the liquid phase.[34] On the other hand, the C=O stretching mode for the chain form in acetic acid solid is usually observed at 1648 cm⁻¹.[35]

Figure 2 shows the FTIR-RA spectrum of acetic acid deposited at 1.0 × 10⁻⁸ Torr (deposition pressure) on the copper disk at 123 K as a function of exposure. The most prominent spectral features have been assigned in accord with the literature data[24,32,34−36] and are listed in Table 1. In particular, at low exposure (Figure 2a,b), the spectrum shows two prominent features at 1716 and 1304 cm⁻¹, which can be attributed to the C=O and C−O stretching modes, respectively. These features are found to shift gradually to higher frequencies at higher

exposures (Figure 2c,d). Furthermore, additional features at 1653, 1436, 1418, and 1363 cm⁻¹ become evident at the 10 L exposure (Figure 2d), and they can be assigned respectively to the C=O stretching mode (of the chain form), COH scissoring mode, and the CH₃ asymmetric and symmetric scissoring modes, in good accord with similar spectral assignments made in the earlier studies for acetic acid solid[35] and for acetic acid adsorbed on Pt (111)[37] and Ru(0001).[24] The new feature at 1792 cm⁻¹ found at higher exposures (Figure 2d) can also be attributed to the C=O stretching mode for acetic acid molecules not participating in the bulk structure, which is similar in frequency to that found for weakly interacting acetic acid monomers (in the gas phase).[32] Given that the CO stretching modes (at 1732 and 1314 cm⁻¹) for the condensed acetic acid film (for higher exposures) are evidently very similar to those of gas-phase acetic acid dimers[34,38] (Table 1), the deposition of acetic acid on the copper disk can therefore be characterized as physical adsorption involving the formation of dimers, as previously observed on Pt (111)[37] and Ru (0001).[24] At lower exposures, these CO features are found at lower frequencies (1716 and 1304 cm⁻¹), indicating the differences in the dimer formation in the first (two) adlayers during the initial stage of film growth (on the copper disk). The relative intensities of the present spectrum for the acetic acid film at high exposure (Figure 2d) are also found to be quite different from those for the solid acetic acid spectrum obtained in the transmission mode,[35] which could be due to the metal surface selection rule and the possible presence of different structures.

Figure 3 shows the thermal evolution of FTIR-RA spectra of 20 L of acetic acid deposited at 1.0 × 10⁻⁸ Torr (deposition pressure) at 123 K. These spectra were collected with the sample held at the preselected temperature as indicated in Figure 3. Evidently, three general trends in the changes of the spectral features can be observed upon annealing the sample from 123 to 173 K. In particular, the most prominent feature, C=O stretch at 1732 cm⁻¹, observed at 123 K (Figure 3a and Figure 2d) is found to gradually reduce in intensity. Furthermore, the weak shoulder at 1712 cm⁻¹ (Figure 3b) appears to evolve into a doublet at 1711 and 1720 cm⁻¹ at 153 K (Figure 3c), which are found to reduce in intensity upon further annealing the

TABLE 1: Comparison of Vibrational Band Frequencies (in cm⁻¹) of Acetic Acid in the Gas Phase, Ar Matrix, Liquid, and Solid Phases, as well as of Acetic Acid Adsorbed on Ru(0001) at 100 K with Those of Acetic Acid Solids As Deposited at 123 K and upon Annealing to 173 K Obtained in the Present Work

band assignment[a]	monomer[b] [refs 32 and 36]	dimer[c] [ref 34]	solid phase [ref 35]	Ru(0001) [ref 24]	solid as deposited at 123 K [this work]	deposit after being annealed to 173 K [this work]
ν(OH)	3583 (3566)	3027 (3028)	2934	3028	3028	
ν_{as}(CH$_3$)	2996	3030		2994	2994	2995
ν(C=O) + δ_s(CH$_3$)			2988			
ν_s(CH$_3$)	3051/2944	3030		2924	2924	2931
δ(COH) + ν_s(CH$_3$)			2760			
ν(C−O) + δ(OH)			2664	2691	2691	2674
ν(C−O) + δ_s(CH$_3$)			2614	2641	2640	2621
2ν(C−O)			2519	2575	2574	2576
ν(C=O)	1788 (1779)	1730 (1715)	1715	1794	1792	1790/1749
			1659	1732	1732	1700
					1653	1660/1646
δ(OCO) + ν(CC)			1520			1529
δ(COH)	1182 (1181)	1422 (1413)	1406	1439	1436	1447
δ_{as}(CH$_3$)	1430 (1439)	1422 (1413)		1418	1418	1423/1412
δ_s(CH$_3$)	1382 (1380)	1365 (1359)	1365	1366	1363	1370/1365
ν(C−O)	1264 (1259)	1292 (1295)	1269	1313	1314	1323/1301
						1284
ρ_{as}(CH$_3$)	1048 (1044)	1060 (1050)	1049	1053		
ρ_s(CH$_3$)	989 (987)	1005 (1013)	1018	1024		
γ(OH)		940 (934)	906	959		
ν(C−C)	847	890 (886)	891			
δ(OCO)	642 (639)	621 (624)	629			
ρ(OCO)	581 (581)		473			
δ(CCO)		475 (480)	449			

[a] Band notations: ν = stretch, δ = scissor, ρ = rock, γ = twist, s = symmetric, as = asymmetric. [b] Data for the gas-phase monomers are compared with those obtained in an Ar matrix shown in parentheses. [c] Data for the gas-phase dimers are compared with those obtained in the liquid phase shown in parentheses.
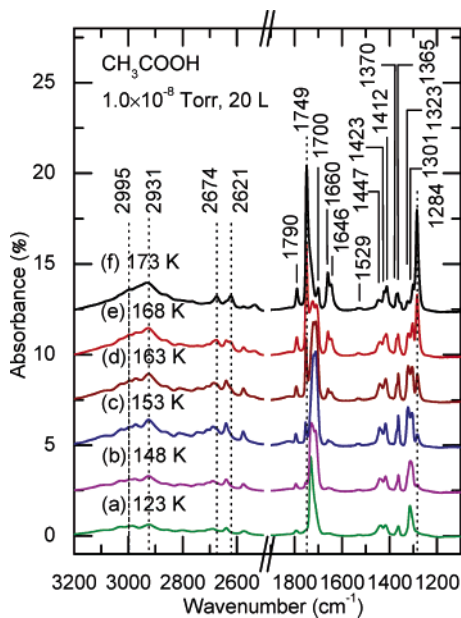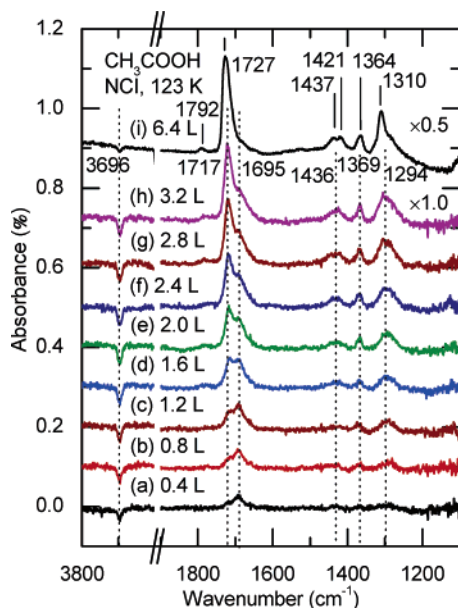

Figure 3. FTIR-RA spectra of 20 L of acetic acid vapor-deposited at 1.0×10^{-8} Torr (a) at 123 K, and upon annealing to (b) 148, (c) 153, (d) 163, (e) 168, and (f) 173 K.

sample to 173 K (Figure 3f). On the other hand, new C=O stretch features at 1660 and 1646 cm⁻¹ are found to increase in intensity during the thermal evolution from 123 to 173 K. Given that the original prominent C=O stretch feature at 1732 cm⁻¹ can be attributed to that of the acetic acid dimers in the noncrystalline solid phase[34] while those at 1660 and 1646 cm⁻¹ could be assigned to bulk polymer in the solid,[35] the intermediate features at 1711 and 1720 cm⁻¹ could therefore be attributed to intermediate (oligomer) structures between the dimer and chain-form polymer structures. The peaking of the intensity of

the doublets of the intermediate structures upon thermal annealing suggests a phase transition of acetic acid from a noncrystalline state to a crystalline state. Furthermore, the weak feature at 1792 cm⁻¹ (Figure 3a and Figure 2d) and the new feature at 1749 cm⁻¹ (Figure 3f) can be attributed to the C=O stretch of acetic acid monomers located on the surface (surface monomers) and of those trapped in the bulk (bulk monomers), respectively, not directly interacting with the bulk structure. The strengthening of both of these monomer C=O stretch features upon annealing the sample to 173 K (Figure 3f) is consistent with the crystallization process.

Similar thermal evolution in the C−O stretch region can also be observed. In particular, the strong C−O stretch feature at 1314 cm⁻¹ at 123 K (Figure 3a and Figure 2d) is found to evolve into a doublet at 1322 and 1306 cm⁻¹ with slightly enhanced intensity at 153 K (Figure 3c), which then undergoes reduction in intensity upon further annealing the sample to 173 K (Figure 3f). These spectral changes are consistent with thermal evolution of the bulk dimer to chain-form polymer, as proposed above. The rapid increase in the intensity of the new feature at 1284 cm⁻¹ in concert with the new C=O stretch feature at 1749 cm⁻¹ with increasing temperature (observed above) can therefore be used to assign the feature at 1284 cm⁻¹ similarly to the C−O stretch of the bulk monomers. The presence of the C−O stretch feature for the surface monomers expected to be above 1284 cm⁻¹ could be hidden by the nearby strong dimer/polymer features, which could contribute to the more complex profile changes found in the C−O stretch region at different annealing temperatures (Figure 3f).

Crystallization from noncrystalline to crystalline acetic acid solid is also evident in the thermal evolution of the symmetric and asymmetric bending modes of the CH₃ group found at 1363 and 1418 cm⁻¹ respectively, as well as the COH bending mode observed at 1436 cm⁻¹ at 123 K (Figure 3a and Figure 2d).

Thermal Evolution of Acetic Acid Nanodeposits

J. Phys. Chem. B, Vol. 109, No. 27, 2005 **13267**

Figure 4. FTIR-RA difference spectra of acetic acid vapor-deposited at 2.0×10^{-9} Torr on a noncrystalline ice (NCI) film at 123 K as a function of acetic acid exposure: (a) 0.4, (b) 0.8, (c) 1.2, (d) 1.6, (e) 2.0, (f) 2.4, (g) 2.8, (h) 3.2 , and (i) 6.4 L.

Figure 5. FTIR-RA difference spectra of acetic acid vapor-deposited at 2.0×10^{-9} Torr on a polycrystalline ice (PCI) film at 123 K as a function of acetic acid exposure: (a) 0.4, (b) 0.8, (c) 1.2, (d) 1.6, and (e) 6.0 L.

Like the C=O stretching mode for the intermediate oligomer forms at 1712 cm^{-1}, these features appear to increase in intensity upon annealing the sample to 153 K (Figure 3c) and then weaken upon further annealing to 173 K (Figure 3f). These changes are less pronounced than those found for the CO stretching modes because these functional groups are not directly involved in intermolecular bonding. Furthermore, the spectral changes in the 2500−2800 cm^{-1} region corresponding to various combination bands and those above 2800 cm^{-1} corresponding to the CH$_3$ stretching modes (at 2924 and 2994 cm^{-1}) and OH stretching mode (at 3028 cm^{-1}) (Figure 2d, Table 1) are more difficult to characterize over the annealing temperature range due to the multitude, broadness, and complexities of many of these features. In particular, the combination band in the 2500−2800 cm^{-1} region appears to reach a maximum near 153 K (Figure 3c), which is consistent with the spectral behavior in the aforementioned crystallization process for some of the constituent functional groups (CO) that are directly involved in the intermolecular bonding. Above 2800 cm^{-1}, the broad spectrum generally increases in intensity upon annealing the sample to 173 K (Figure 3f). Finally, it is important to note that the crystallization process of acetic acid is irreversible, i.e., the spectrum collected with the acetic acid film held at 173 K (Figure 3f) remains unchanged after the film was re-cooled back to 123 K. This crystallization process is therefore similar to that found for transformation from NCI to PCI as demonstrated in our recent work.[29]
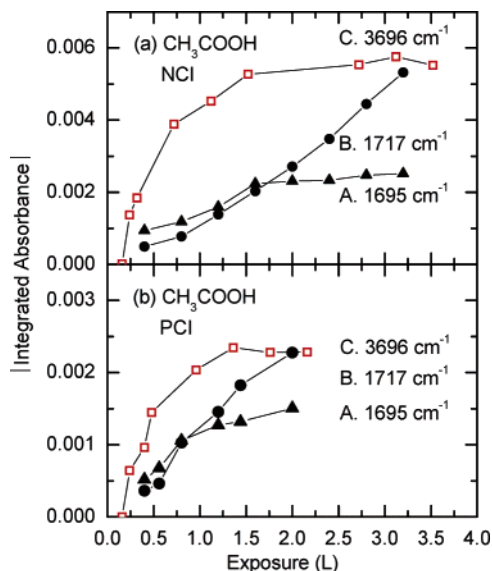
3.3. Adsorption of Acetic Acid on Noncrystalline and Polycrystalline Ice Films. Figures 4 and 5 shows the FTIR-RA difference spectra of acetic acid vapor-deposited at 2.0×10^{-9} Torr (deposition pressure) as a function of exposure on NCI and PCI films (approximately 6 nm thick), respectively. The difference spectra were obtained by subtracting the FTIR-RA spectra of the corresponding pristine NCI or PCI film from the sample spectra. It should be noted that the choice of the ice film thickness was arbitrary but the present thickness (i.e., 6 nm) appears to be large enough to provide a sufficient proportion of OH dangling bonds for the present investigation. At sub-monolayer exposure (Figure 4a), the C=O stretching mode
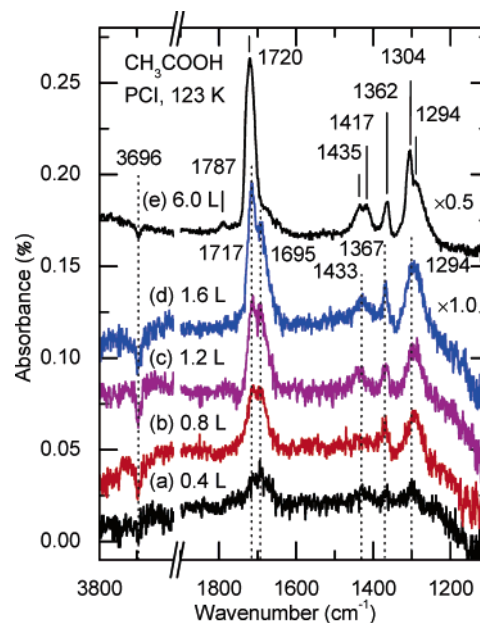
evidently emerges as a weak profile consisting of two components at 1717 and 1695 cm^{-1}. As the exposure is increased, the relative intensity of the component feature at 1717 cm^{-1} is found to overtake that of the feature at 1695 cm^{-1}, with the latter saturating at 1.2 L exposure (Figure 4c). Concomitantly, the intensity of the OH dangling-bond feature at 3696 cm^{-1} is found to decrease with increasing exposure (Figure 4a−c). Above 1.2 L, no further increase in the intensity of the C=O stretch feature at 1695 cm^{-1} nor decrease in that of the OH dangling-bond feature at 3696 cm^{-1} with increasing exposure are observed (Figure 4d−h). The strong inverse correlation in intensity between the C=O stretch feature at 1695 cm^{-1} and the OH dangling-bond feature at 3696 cm^{-1} at low exposure strongly suggests that the C=O stretch feature at 1695 cm^{-1} corresponds to the formation of a surface complex of acetic acid (monolayer) with the dangling bonds of the ice film. On the other hand, the C=O stretch feature at 1717 cm^{-1} is found to strengthen further with increasing exposure, suggesting that this feature could be attributed to acetic acid in multilayers. In addition, the C−O stretch feature at 1294 cm^{-1}, and the symmetric and asymmetric CH$_3$ bending modes at 1369 and 1436 cm^{-1}, respectively, are found to increase in intensity with increasing exposure (Figure 4). Unlike the C=O stretching feature at 1695 cm^{-1}, saturation of these features related to monolayer bonding is not observed, which suggests that the OH dangling bond of the ice surface does not strongly interact with the C−O and CH$_3$ constituent groups.

The FTIR-RA difference spectra for acetic acid on PCI (Figure 5) are found to exhibit similar vibrational features for acetic acid with similar frequencies as those found on NCI (Figure 4). These spectra also follow a similar trend with increasing exposure as that found for acetic acid on NCI (Figure 4). In particular, the increase in the C=O stretching mode at 1695 cm^{-1} is also found to correlate with a concomitant reduction in the OH dangling-bond signal at 3696 cm^{-1} for submonolayer exposures (Figure 5a−d), again supporting our hypothesis that the C=O stretch feature at 1695 cm^{-1} corresponds to interactions of acetic acid in the first monolayer with the ice surface. The lack of saturation of the other C=O stretch

Figure 6. Profiles of the magnitudes of integrated absorbance of FTIR-RA difference spectral features at (A) 1695 (▲), (B) 1717 (●), and (C) 3696 cm^{-1} (□) of acetic acid deposited at 2.0×10^{-9} Torr as a function of acetic acid exposure on (a) noncrystalline ice (NCI) and (b) polycrystalline ice (PCI) at 123 K.

Figure 7. FTIR-RA difference spectra of 3.2 L of acetic acid vapor-deposited at 2.0×10^{-9} Torr on a noncrystalline ice (NCI) film at 123 K as a function of annealing temperature: (a) 128, (b) 139, (c) 155, (d) 158, (e) 161, (f) 164, (g) 168, and (h) 174 K.

feature at 1717 cm^{-1} can therefore be attributed to acetic acid in multilayer adsorption. Moreover, the C–O stretch at 1294 cm^{-1} and the symmetric and asymmetric bending modes of CH$_3$ at 1433 and 1367 cm^{-1}, respectively, are also found to increase in intensity with increasing exposure (Figure 5a–d), which also indicates weak interactions between these constituent groups with ice.

Further exposure of acetic acid to PCI (Figure 5e) and to NCI (Figure 4i) at 123 K to ~6 L produces difference spectra similar to that of acetic acid solid film (Figure 2c), which shows that the effect of the substrate is no longer important for the thicker acetic acid film. At higher exposure, the small but discernible blue shift of the C=O stretch from 1717 cm^{-1} for 1.6 L (Figure 5d) to 1720 cm^{-1} for 6.0 L exposure (Figure 5e) is found to be consistent with the continued build up of the multilayer with increasing exposure on PCI, as observed similarly for acetic acid solid film (Figure 2) and for acetic acid on NCI [e.g., from 1717 cm^{-1} for 3.2 L (Figure 4h) to 1727 cm^{-1} for 6.4 L (Figure 4i)].

We have estimated the spectral intensities of the two C=O features and the OH dangling-bond features by a nonlinear least-squares fitting procedure involving primarily Gaussian mixed with Lorentzian line shapes, and the corresponding integrated absorbance profiles as a function of acetic acid exposure on NCI and PCI are shown in Figure 6. These profiles show that the adsorption of acetic acid on NCI and PCI follows a similar pattern, in which the acetic acid molecule binds to the ice surface through interactions between C=O and the OH dangling bond during the early stage of adsorption (i.e. before complete adsorption of a monolayer). The increase in the intensity of the monolayer C=O stretch feature at 1695 cm^{-1} (Figure 6, curves A) appears to level off near 1.2 L, while that for the multilayer C=O stretch feature at 1717 cm^{-1} (Figure 6, curves B) continues to increase with increasing exposure. The lower magnitude of the depleted dangling-bond signal for saturation adsorption on PCI than that on NCI is consistent with the relative number of OH dangling bonds on the PCI and NCI films. Furthermore, the slightly lower saturation exposure of acetic acid for PCI (0.7 L) relative to that for NCI (0.9 L) indicates a lower proportion of acetic acid per dangling-bond interaction for PCI
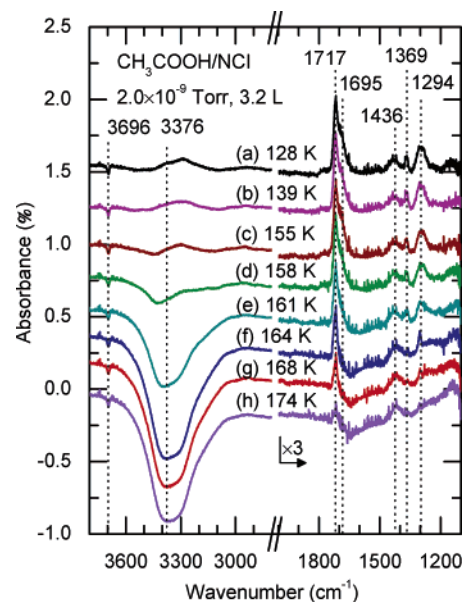
than NCI, suggesting that there are fewer dangling-bond sites available for bonding with acetic acid on PCI than NCI. (The saturation exposures were estimated from the respective curves in Figure 6 by the intercepts of two straight lines drawn from the 3–4 points at the low and high exposure sides.) It should be noted that examination of the ice spectral region before and after the adsorption of acetic acid shows complete extinction of the dangling-bond signal upon complete adsorption of the first monolayer. Furthermore, the presence of the C=O stretching mode corresponding to multilayer adsorption is discernible even at the lowest exposure employed in the present work, which would suggest that island formation has already occurred before the completion of the first monolayer adsorption of acetic acid.

3.4. Thermal Evolution of Acetic Acid on Noncrystalline and Polycrystalline Ice Films. Figures 7 and 8 show the thermal evolution of the FTIR-RA difference spectra of 3.2 and 1.8 L of acetic acid vapor-deposited at 2.0×10^{-9} Torr (deposition pressure) respectively on NCI and PCI films (approximately 6 nm thick). The difference spectra were obtained by subtracting the FTIR-RA spectra of the corresponding pristine NCI (Figure 1a) or PCI film (Figure 1e) obtained at 123 K from the sample spectra collected at a preselected sample temperature (indicated in Figures 7 and 8). Evidently, the intensity of the monolayer C=O stretch feature at 1695 cm^{-1} appears to decrease with increasing temperature and become totally diminished at 164 K (Figure 7f), while the intensity of the more prominent multilayer C=O stretch feature at 1717 cm^{-1} remains essentially unchanged from 128 (Figure 7a) to 164 K (Figure 7f). This multilayer C=O stretch feature weakens with increasing temperature only after the extinction of the monolayer C=O stretch feature above 164 K. Furthermore, thermal evolution of the COH bending feature at 1436 cm^{-1}, the CH$_3$ bending features at 1369 cm^{-1}, and the C–O stretch feature at 1294 cm^{-1} follow that of the multilayer C=O stretch, confirming that these vibrational modes contain predominant contributions from the multilayer component of the acetic acid film. However, the C–O stretch feature at 1294 cm^{-1} becomes markedly sharpened at 164 K, which suggests that the depleted component located at the lower frequency near 1284 cm^{-1} is related to the monolayer component and therefore should follow

Thermal Evolution of Acetic Acid Nanodeposits

J. Phys. Chem. B, Vol. 109, No. 27, 2005 **13269**
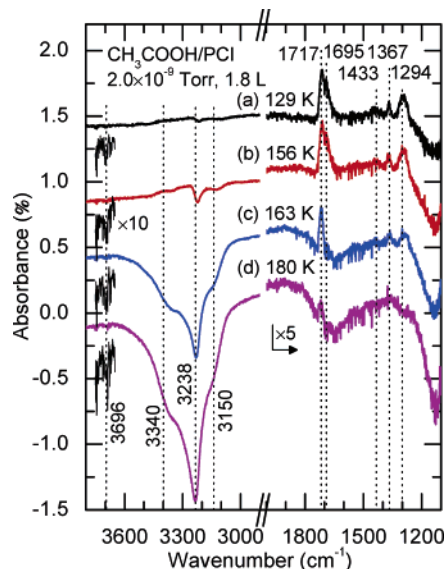
Figure 8. FTIR-RA difference spectra of 1.8 L of acetic acid vapor-deposited at 2.0×10^{-9} Torr on a polycrystalline ice (PCI) film at 123 K as a function of annealing temperature: (a) 129, (b) 156, (c) 163, and (d) 180 K.

Figure 9. Profiles of the magnitudes of integrated absorbance of FTIR-RA difference spectral features at (A) 1695 (▲), (B) 1717 (●), (C) 3380/3240 (□), and (D) 3696 cm^{-1} (○) of 3.2 and 1.8 L of acetic acid vapor-deposited at 2.0×10^{-9} Torr as a function of annealing temperature on respectively (a) noncrystalline ice (NCI) and (b) polycrystalline ice (PCI) at 123 K.

similar thermal evolution as that of the C=O stretch feature at 1695 cm^{-1}. In addition, minor reduction in the intensity and minor change in the shape of the OH stretch feature near 3376 cm^{-1} are found upon annealing the sample from 128 (Figure 7a) to 158 K (Figure 7d). However, we did not observe the shape normally expected for a PCI film near 160 K (Figure 1e), which indicates that the transformation from NCI to PCI (Figure 1) has not occurred. Moreover, further annealing the sample to 164 K caused major depletion in the intensity of the OH stretch of the NCI film (Figure 7f), which appears to correlate well with the complete depletion of the first-monolayer C=O stretch feature at 1695 cm^{-1}. The presence of acetic acid with strong H-bonding interaction on the ice surface therefore appears to not only prevent crystallization of the NCI film, but also induce coevaporation of acetic acid with water. Annealing the sample (from 164 K) further to 174 K appears to cause reduction in the remaining acetic acid, after complete evaporation of the NCI film. Furthermore, the OH dangling-bond feature at 3696 cm^{-1} has been completely quenched upon exposure of acetic acid above 1.2 L, as illustrated in Figure 4. No significant change in this feature is found upon thermal annealing from 128 to 174 K (Figure 7), which further supports the strong H-bonding interaction between acetic acid and water in the interface (first-monolayer) region.

The thermal evolution of 1.8 L of acetic acid on the PCI film (Figure 8) follows a similar trend as that of 3.2 L of acetic acid on the NCI film (Figure 7). In particular, the reduction in the intensity of the monolayer C=O stretch feature at 1695 cm^{-1} from 129 K (Figure 8a) to 163 K (Figure 8c) is followed by reduction in that of the multilayer C=O stretch feature at 1717 cm^{-1} at a higher temperature (180 K, Figure 8d). The changes in the intensity of the multilayer C=O stretch with increasing temperature are similar to those of the COH bending feature at 1433 cm^{-1}, the CH$_3$ bending features at 1367 cm^{-1}, and the C−O stretch feature at 1294 cm^{-1}. The immediate quenching of the dangling-bond feature at 3696 cm^{-1} upon adsorption of acetic acid supports the strong H-bonding interaction between acetic acid and water observed also for the NCI film. The PCI film clearly exhibits the characteristic OH stretch profile, with the maximum at 3238 cm^{-1} (Figure 8). The gradual depletion
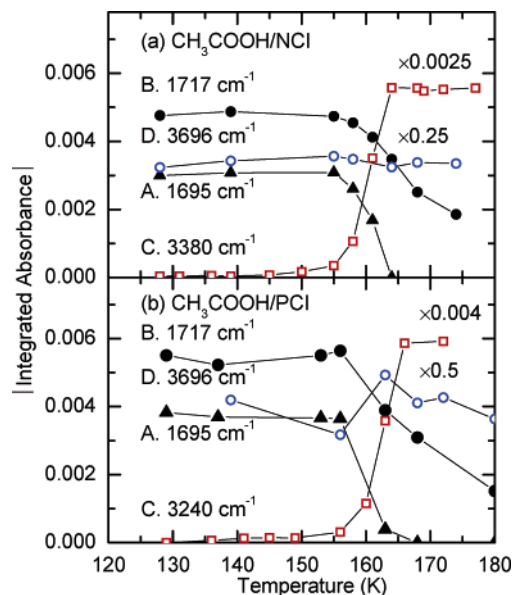
of the intensity of this feature with increasing temperature to 163 K (Figure 8c), in concert with the reduction in that of the monolayer C=O stretch feature at 1695 cm^{-1}, again indicates water coevaporating with acetic acid (likely as an acetic acid hydrate). This coevaporation continues until the complete PCI film has been exhausted, after which evaporation of the remaining acetic acid solid film continues to proceed with increasing temperature. As with the adsorption of a low exposure of acetic acid on the NCI film, the acetic acid adsorbed on the PCI film does not appear to exhibit crystallization upon annealing above 153 K (the on-set of crystallization observed in Figure 3). The lack of transformation to a crystalline state is likely due to the relatively small amount of acetic acid adsorbed on the NCI and PCI films.

Our proposed picture for the thermal evolution of acetic acid on NCI and PCI films can be summarized by the integrated absorbance profiles of the monolayer and multilayer C=O stretching modes, OH stretching, and OH dangling-bond features as a function of temperature, shown in Figure 9. Integrated absorbance is estimated by integrating the absolute magnitude of the absorbance over the vibrational feature of interest in the respective difference spectra (Figures 7 and 8). The monolayer and multilayer C=O features at 1695 and 1717 cm^{-1}, respectively, have been fitted with Gaussian−Lorentzian line shapes in order to determine the corresponding integrated absorbance. Between 125 and 155 K, all of the integrated absorbance profiles remain flat, indicating little change in the intensity of the respective features. Water evaporation is clearly marked by the on-set of the increased depletion in the intensity of the OH stretching feature of water (Figure 9, curves C) at 155 K on the NCI and PCI films, while the integrated absorbances of both monolayer (Figure 9, curves A) and multilayer C=O features (Figure 9, curves B) of the adsorbed acetic acid are found to decrease correspondingly. Furthermore, the integrated absorbance profiles of the OH stretching feature (Figure 9, curves C) are found to level off at 164 K, indicating complete evaporation of the ice substrate. Correspondingly, the integrated absorbances of the monolayer C=O features of acetic acid at

1695 cm^{-1} on NCI and PCI films (Figure 9, curves A) are both reduced to zero from 155 to 164 K, providing evidence for water coevaporation with acetic acid in the interface region. The gradual reduction in the integrated absorbances of the multilayer C=O features of acetic acid at 1717 cm^{-1} on both NCI and PCI films (Figure 9, curves B) from 155 K to above 164 K is consistent with the coevaporation picture and the continued evaporation of acetic acid after complete depletion of the ice film. Moreover, the rate of reduction of the multilayer C=O feature at 1717 cm^{-1} with increasing temperature is found to be smaller than that of the monolayer C=O feature at 1695 cm^{-1} (as indicated by the slopes of the corresponding profiles) above 155 K for both NCI and PCI films (Figure 9), suggesting that the interactions among acetic acid molecules are stronger than those between acetic acid and water (i.e. those found in the first monolayer). During the thermal evolution, the integrated absorbance of the OH dangling-bond feature of water at 3696 cm^{-1} (Figure 9, curves D) remains unchanged for both NCI and PCI samples, indicating that the initial adsorption of acetic acid on ice has consumed all the dangling bonds and therefore no further reduction is possible upon further annealing.

We have also conducted a similar study on the thermal evolution of the corresponding FTIR-RA difference spectra for a higher exposure of acetic acid (>6 L) deposited on NCI and PCI films at 123 K. The as-deposited spectra (not shown) are dominated by the intense multilayer C=O stretching features at 1732 cm^{-1} at 123 K. Similar to the case of low acetic acid exposure shown in Figures 7 and 8, water coevaporation with acetic acid is again found to begin at 155 K and continue until complete exhaustion of the ice film at about 165 K. Further annealing the sample above 165 K produces crystallization of the remaining acetic acid, as indicated by the emergence of the characteristic bulk monomer C=O stretch feature at 1749 cm^{-1} and the C–O stretch feature at 1284 cm^{-1}. The corresponding spectral evolution with increasing temperature for both NCI and PCI samples (not shown) follows that of a solid acetic acid film above 165 K (similar to those shown in Figure 3e,f). During the course of thermal evolution, we did not observe conversion of the NCI substrate to the PCI substrate before complete water evaporation has occurred. This observation suggests that the interactions between acetic acid and water are sufficiently strong that the presence of acetic acid may therefore prevent the initiation of crystallization of an ultrathin NCI film (<6 nm thick). For a thicker NCI film (with thickness greater than 10 nm), crystallization of NCI film has been found to proceed as expected even with the adsorption of acetic acid.

4. Concluding Remarks

In summary, FTIR-RA spectra have been collected for pristine solid acetic acid films and acetic acid adsorbed on ultrathin films of NCI and PCI at 123 K, and spectral evolution upon annealing the sample to 180 K has also been obtained in the present work. In particular, acetic acid vapor-deposited at 123 K is found to exist as an amorphous solid, which undergoes a phase transformation to a more structurally ordered (polycrystalline) form between 153 and 173 K. Two prominent C=O stretching features were observed for acetic acid adsorbed on NCI and PCI films at 123 K, and they could be attributed to the H-bonded species between C=O and the OH dangling bond in the first monolayer (1695 cm^{-1}) and to those upon the subsequent formation of multilayers (1717 cm^{-1}). The evidence of multilayer formation suggests possible formation of acetic acid islands on these NCI and PCI films. For a low exposure of acetic acid

on 6-nm-thick NCI and PCI films, acetic acid is found to undergo coevaporation with water likely as an acetic acid hydrate at 155 K, which continues until the entire ice film (substrate) has been exhausted at 165 K. Above 165 K, the remaining acetic acid solid appears to evaporate without undergoing the aforementioned phase transformation to a more structurally ordered form, in contrast to the case of a high acetic acid exposure (>6 L). Furthermore, coevaporation of acetic acid with water is found to proceed at a faster rate than the subsequent evaporation of acetic acid alone, which is consistent with the weaker interactions found in the H-bonded acetic acid–water complex than that in acetic acid solids.

It is of interest to compare the present FTIR-RA spectra of acetic acid on NCI and PCI with other adsorbates. In particular, in the case of the adsorption of acetone on NCI and PCI, Schaff and Roberts[12,39] and Mitlin and Leung[19] reported observation of two prominent C=O stretching features at similar frequencies, 1703 and 1717 cm^{-1}, which can be attributed to H-bonded acetone and physisorbed (multilayer) acetone, respectively. Furthermore, Schaff and Roberts[39] also observed the depletion of the multilayer feature at 1717 cm^{-1} before the H-bonded feature at 1703 cm^{-1} upon annealing acetone adsorbed on NCI to 175 K, in marked contrast to the thermal evolution behavior of the corresponding features for acetic acid on NCI as observed in the present work. The acetone–acetone interactions are therefore weaker than acetone–water interactions. The presence of the hydroxyl group produces additional H-bonding opportunity and stronger intermolecular interactions in acetic acid. The replacement of the methyl group by the hydroxyl group as in acetic acid therefore has a significant effect on the respective chemical and physical properties of acetone and acetic acid on ice films. Furthermore, similar frequencies have also been observed for other vibrational modes for the adsorption of acetone and of acetic acid on NCI and PCI,[39] further supporting the interactions between C=O and the OH dangling bond as the primary adsorption mechanism for both adsorbates.

The present work provides the first infrared spectroscopic data for the adsorption of an organic acid on ice between 123 and 180 K. Hudson et al. have investigated the uptake of acetone, acetaldehyde, and acetic acid on ice films in nearly the same temperature region (130–180 K) as the present study by using mass spectrometric techniques.[20] Of interest to the present work is that acetic acid has also been found to be more tightly bound on ice than acetone at the lower temperature end by Hudson et al., consistent with our observation that acetic acid evaporates at a higher temperature than acetone.[20] Solokov and Abbatt extended the uptake study of acetic acid (and n-alcohols and hexanal) on ice to 213–245 K and concluded among other observations that the ice surface in this temperature region behaves more like liquid than solid.[21] Extension of the present spectroscopic study to this higher temperature regime would therefore be of great interest to further characterize the role of H-bonding interactions in these adsorption studies. Not surprisingly, the adsorption behavior of small inorganic acids such as HCl and HBr on ice[18,40,41] is found to be rather different from that observed in the present work. In particular, HCl was found to form a bound molecular state on the ice surface below 50 K and to penetrate into ice above 60 K, where it subsequently dissociates as ions converting the ice to amorphous and crystalline hydrates respectively below and above 140 K.[18,40] In addition, Hanson and Ravishankara also showed that the adsorption of HBr was as efficient as HCl on the ice surface, while HF was only weakly taken up by ice.[41] In contrast, no experimental evidence for the penetration and ionization of

Thermal Evolution of Acetic Acid Nanodeposits

J. Phys. Chem. B, Vol. 109, No. 27, 2005 **13271**

acetic acid upon adsorption on NCI and PCI has been obtained under the present experimental conditions between 123 and 180 K.

The FTIR-RA spectra of acetic acid adsorbed on the Ru(0001) surface at 100 K have been reported by Garcia et al.[24] and found to be quite similar to the present data for acetic acid on NCI and PCI. With the exception of the C=O stretching feature at 1695 cm^{-1} (corresponding to the acetic acid H-bonded to ice), the observed spectral similarities for the two substrates therefore indicate that the adsorption states of acetic acid on NCI and PCI could be considered as molecular and physisorbed states as those found for Ru(0001) at 100 K.[24] The difference between metal and ice surfaces is mainly attributed to the presence of the OH dangling bond on the ice surface. The adsorption of acetic acid on other metal surfaces, including Pt(111),[37] Cu(100),[42] Rh(111),[43] and Pd(110),[44] has also been reported. Like the adsorption of acetic acid on Ru(0001) above 100 K, evidence of dehydrogenation and formation of acetate has been obtained for these metal surfaces at different temperatures and coverage.

Compoint et al. have studied the geometry and dynamics of acetic acid and formic acid adsorbed on/in ice by classical molecular dynamics simulation at 250 K.[23] Unfortunately, no simulation in the temperature region employed in the present work (123−180 K) and that of interest to ozone depletion (190−220 K) have been reported for these systems, which could provide valuable information about the structural evolution upon annealing, formation of contact ion pairs ($CH_3COO^- - H_3O^+$), and other adsorption phenomena on ice.[1] Furthermore, quantum mechanical computations of model adsorbate−ice systems have thus far been limited to small adsorbates such as HCl, HF, and HBr.[45,46] Despite the usual limitations of these quantum computations, these calculations could provide qualitative insights into the larger oxygenated hydrocarbons (such as acetic acid). Our recent calculations on acetic acid monohydrate and dihydrate using the density functional method have provided support for the observed trends in the relative strengths of the H-bonding interactions among water, acetic acid, and their hydrates.[47] The present spectroscopic data are expected to stimulate further computational studies of larger systems to improve our understanding of the intricate phenomena of oxygenated hydrocarbons on ice and of their associated H-bonding interactions.

References and Notes

(1) Girardet, C.; Toubin, C. *Surf. Sci. Rep.* **2001**, *44*, 159.
(2) Sanford, S. A. Polarimetry of the interstellar medium. *Astron. Soc. Pac. Conf. Series* **1996**, *97*, 29.
(3) Solomon, S. *Rev. Geophys.* **1988**, *26*, 131.
(4) Fan, S. M.; Jacob, D. J. *Nature* **1992**, *359*, 522.
(5) Finlayson-Pitts, B. J.; Livingston, F. E.; Berko, H. N. *Nature* **1990**, *343*, 622.
(6) Brasseur, G.; Granier, C. *Science* **1992**, *257*, 1239.
(7) Hofmann, D. J.; Solomon, S. J. *J. Geophys. Res.* **1989**, *94*, 5029.
(8) Zellner, R. *Global Aspects of Atmospheric Chemistry*; Springer: New York, 1999.
(9) Seinfeld, J. H.; Pandis, S. N. *Atmospheric Chemistry and Physics*: *From Air Pollution to Climate Change*; Wiley: New York, 1998.
(10) Devlin, J. P. *J. Phys. Chem.* **1992**, *96*, 6185.
(11) Horn, A. B.; Chesters, M. A.; McCoustra, M. R. S.; Sodeau, J. R. *J. Chem. Soc., Faraday Trans.* **1992**, *88*, 1077.
(12) Schaff, J. E.; Roberts, J. T. *J. Phys. Chem.* **1994**, *98*, 6900.
(13) Rowland, B.; Fisher, M.; Devlin, J. P. *J. Chem. Phys.* **1991**, *95*, 1378.
(14) Kuhs, W. F.; Lehmann, M. S. *Water Sci. Rev.* **1986**, *2*, 1.
(15) Buch, V.; Devlin, J. P. *J. Chem. Phys.* **1991**, *94*, 4091.
(16) Rowland, B.; Devlin, J. P. *J. Chem. Phys.* **1991**, *94*, 812.
(17) Andrews, L.; Arlinghaus, R. T.; Johnson, G. L. *J. Chem. Phys.* **1983**, *78*, 6347.
(18) Delzeit, L.; Rowland, B.; Devlin, J. P. *J. Phys. Chem.* **1993**, *97*, 10312.
(19) Mitlin, S.; Leung, K. T. *Surf. Sci.* **2002**, *505*, L227.
(20) Hudson, P. K.; Zondlo, M. A.; Tolbert, M. A. *EOS, Transactions* **1999**, *80*, S75.
(21) Sokolov, O.; Abbatt, J. P. D. *J. Phys. Chem. A* **2002**, *106*, 775.
(22) Guerinot, G. Ph.D. Thesis, Université Joseph Fourier, Grenoble, France, 2000.
(23) Compoint, M.; Toubin, C.; Picaud, S.; Hoang, P. N. M.; Girardet, C. *Chem. Phys. Lett.* **2002**, *365*, 1.
(24) Garcia, A. R.; da Silva, J. L.; Ilharco, L. M. *Surf. Sci.* **1998**, *415*, 183.
(25) Mitlin, S.; Leung, K. T. *J. Phys. Chem. B* **2002**, *106*, 6234.
(26) Whalley, E. *Can. J. Chem.* **1977**, *55*, 3429.
(27) Ataka, K.; Yotsuyanagi, T.; Osawa, M. *J. Phys. Chem.* **1996**, *100*, 10664.
(28) Bertie, J. E.; Labbe, H. J.; Whalley, E. *J. Chem. Phys.* **1969**, *50*, 4501.
(29) Mitlin, S.; Leung, K. T. *Can. J. Chem.* **2004**, *82*, 978.
(30) Bertagnolli, H. *Chem. Phys. Lett.* **1982**, *93*, 287.
(31) Bellamy, L. J.; Lake, R. F.; Pace, R. J. *Spectrochim. Acta* **1963**, *19*, 443.
(32) Haurie, M.; Novak, A. *J. Chim. Phys.* **1965**, *62*, 137.
(33) Krause, P. F.; Katon, J. E.; Rogers, J. M.; Phillips, D. B. *Appl. Spectrosc.* **1977**, *31*, 110.
(34) Haurie, M.; Novak, A. *J. Chim. Phys.* **1965**, *62*, 146.
(35) Haurie, M.; Novak, A. *Spectrochim. Acta* **1965**, *21*, 1217.
(36) Berney, C. V.; Redington, R. L.; Lin, K. C. *J. Chem. Phys.* **1970**, *53*, 1713.
(37) Gao, Q.; Hemminger, J. C. *J. Electron Spectrosc. Related Phenom.* **1990**, *54/55*, 667.
(38) Yokoyama, I.; Miwa, Y.; Machida, K. *Bull. Chem. Soc. Jpn.* **1992**, *65*, 746.
(39) Schaff, J. E.; Roberts, J. T. *Langmuir* **1998**, *14*, 1478.
(40) Delzeit, L.; Rowland, B.; Devlin, J. P. *J. Phys. Chem.* **1993**, *97*, 10312.
(41) Hanson, D. R.; Ravishankara, A. R. *J. Phys. Chem.* **1992**, *96*, 9441.
(42) Sexton, B. A. *Chem. Phys. Lett.* **1979**, *65*, 3, 469.
(43) Hoogers, G.; Papageorgopoulos, D. C.; Ge, Q.; King, D. A. *Surf. Sci.* **1995**, *340*, 23.
(44) Aas, N.; Bowker, M. *J. Chem. Soc., Faraday Trans.* **1993**, *89*, 1249.
(45) Calatayud, M.; Courmier, D.; Minot, C. *Chem. Phys. Lett.* **2003**, *369*, 287.
(46) Al-Halabi, A.; Bianco, R.; Hynes, J. T. *J. Phys. Chem. A* **2002**, *106*, 7639.
(47) Gao, Q.; Leung, K. T. *J. Chem. Phys.* **2005**, in press.